1989ApJ...345..906M

THE ASTROPHYSICAL JOURNAL, 345:906–917, 1989 October 15
© 1989. The American Astronomical Society. All rights reserved. Printed in U.S.A.

YOUNG STELLAR OBJECTS IN THE MONOCEROS OB1 MOLECULAR CLOUD

MICHAEL MARGULIS, CHARLES J. LADA, and ERICK T. YOUNG
Steward Observatory, University of Arizona
Received 1988 October 31; accepted 1989 April 13

ABSTRACT

We present detailed results of an *IRAS* survey of a large portion of the Monoceros OB1 (NGC 2264) molecular cloud for discrete far-infrared sources. Using somewhat conservative selection criteria, 30 discrete *IRAS* (25 μm) sources were identified within the same portion of this GMC which already had been systematically surveyed for high-velocity molecular gas by Margulis and Lada. The majority of these sources were detected in at least three of the four *IRAS* bands. About two-thirds of the sources were found to be extended relative to an *IRAS* beamwidth in one or more of the *IRAS* bands. For most of these sources the extended emission is likely to be the result of the superposition of two or more far-infrared emitting objects within a single *IRAS* beam. *IRAS* spectral energy distributions were constructed for 27 of the 30 sources. Although many sources are multiple, most could be fitted into a spectral classification system for young stellar objects based on the shapes of their spectral energy distributions. Eighteen *IRAS* sources were found to have class I energy distributions, characteristic of deeply embedded/protostellar objects. Eight *IRAS* sources were found to have class II energy distributions, typical of partially obscured T Tauri stars with circumstellar disks. Two *IRAS* sources had class III energy distributions, characteristic of normal stellar photospheres, and two *IRAS* sources could not be classified. The presence of many bright class I sources in the Mon OB1 cloud indicates that active star formation is still occurring in the complex which produced the visible cluster, NGC 2264. Our data are consistent with a roughly constant rate of star formation in this complex over the last 3×10^6 yr.

Far-infrared luminosities were calculated for each source by integrating its *IRAS* energy distribution. Class I sources were found to comprise almost all of the luminous (i.e., $L_{bol} > 100\ L_\odot$) pre–main-sequence objects in the Mon OB1/NGC 2264 complex. The lack of class II sources with similarly large bolometric luminosities might suggest the presence of an additional source of luminosity for many of the class I objects. This excess luminosity would most likely be the product of the thermalization of gravitational potential energy at an accretion shock where material in an infalling circumstellar envelope collides with an embryonic stellar core and its surrounding disk. On the other hand, it is also possible (and more likely) that the lack of luminous class II sources is a result of the fact that pre–main-sequence evolution for luminous stars occurs on a time scale comparable to the dissipation time scale for their protostellar (class I) envelopes. Thus, by the time a star has shed its circumstellar gas and dust and become visible it has already arrived on or near the main sequence and has a class III energy distribution.

The region surveyed for discrete *IRAS* sources has also been completely surveyed for high-velocity molecular gas. We find that 50% of the *IRAS* sources in the cloud with $L_{bol} \geq 50\ L_\odot$ are positionally associated with high-velocity molecular gas. Based on statistical arguments it seems likely that the high-velocity molecular gas is physically associated with *IRAS* sources. Assuming that the high-velocity gas is all due to outflows, we derive a lower limit to the birthrate of outflow driving sources in the solar neighborhood of 3×10^{-5} kpc^{-2} yr^{-1}. Our data also suggest that molecular outflow is primarily associated with the earliest stages of pre–main-sequence and protostellar evolution.

Subject headings: infrared: sources — nebulae: individual (Mon OB1) — stars: pre–main-sequence

I. INTRODUCTION

As part of an ongoing study of the global star-formation activity in the Monoceros OB1 molecular cloud complex, the first survey of nearly an entire molecular cloud for both far-infrared sources and molecular outflows has now been completed (Margulis and Lada 1986). Detailed follow-up studies of the outflows in the cloud have now also been made (Margulis, Lada, and Snell 1988). Herein, we present detailed follow-up studies of the far-infrared sources in the cloud. Together, the survey and follow-up studies comprise a detailed road map of the global star-formation activity throughout much of the Monoceros OB1 molecular cloud. In particular, these studies allow us to address the questions of where stars are forming in the molecular cloud at the present epoch, how the various types of young stellar objects in the cloud are related, and which young stars or ptotostars are associated with outflow. In addition, they allow us to construct an evolutionary picture for young stellar objects in the Monoceros OB1 molecular cloud. In this paper, we address these issues and contrast the properties of young stellar objects as they pass through the various stages of protostellar and early stellar evolution.

II. DATA REDUCTION AND RESULTS

This study is primarily concerned with discrete far-infrared sources in the Monoceros OB1 molecular cloud. In order to identify such sources we have constructed co-added maps of emission from the region at 12, 25, 60, and 100 μm from the *IRAS*[1] data base (Beichman *et al.* 1985). The resolutions of the

[1] The *Infrared Astronomical Satellite* was developed and operated by the Netherlands Agency for Aerospace Programs (NIVR), the US National Aeronautics and Space Administration (NASA), and the UK Science and Engineering Research Council (SERC).

© American Astronomical Society • Provided by the NASA Astrophysics Data System

1989ApJ...345..906M

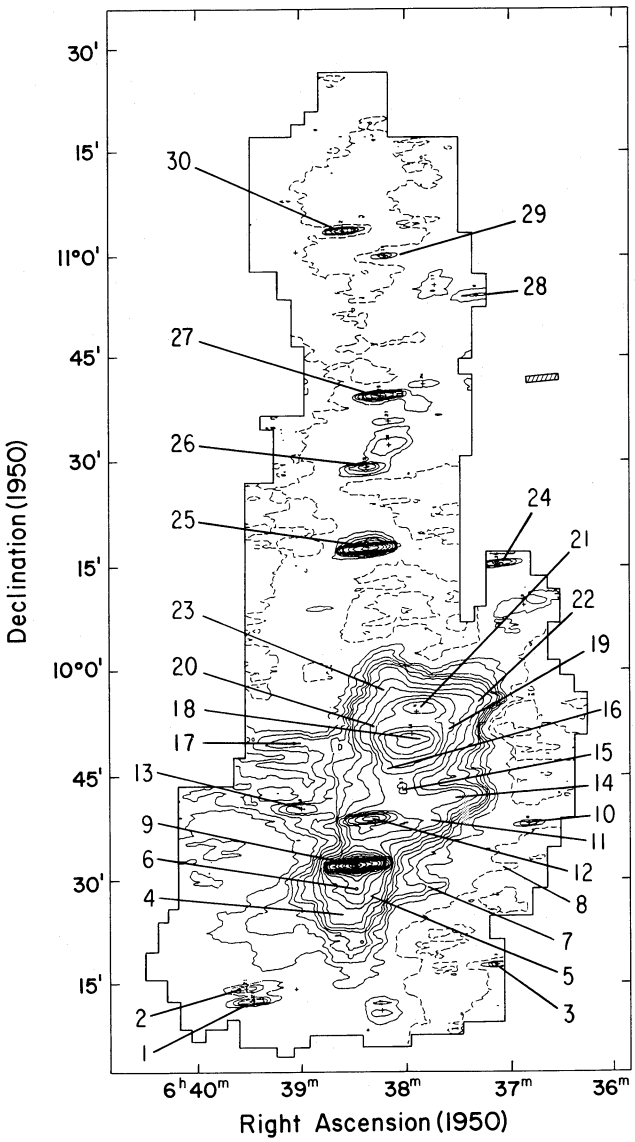

FIG. 1.—Contour map of the intensity of 25 μm *IRAS* emission in the region surveyed for far-infrared sources. Contour levels are at −50.0, −45.0, −40.0, −35.0, −30.0, −25.0, −20.0, −15.0, −12.0, −9.0, −6.0, −3.0, 3.0, 6.0, 9.0 12.0, 15.0, 20.0, 28.3, 40.0, 56.6, 80.0, 113.1, 160.0, 226.3, 320.0, 452.5, 639.9, 905.0, 1279.8, 1810.0, 2559.6, 3619.9, 5119.2, 7239.6, 10238.2, 14478.8, 20476.0, 28957.1, and 40951.1 times a base level of 2.2×10^5 Jy sr^{-1}. Solid contours represent positive intensity levels, while dashed contours represent negative intensity levels. The *IRAS* beam at 25 μm is shown as a hatchmarked box in the figure. The positions of the 30 discrete infrared sources identified in the regions are noted.

co-added maps are 0.′76 × 4.′45 at 12 μm, 0.′76 × 4.′65 at 25 μm, 1.′51 × 4.′75 at 60 μm, and 3.′03 × 5.′05 at 100 μm. An example of such a map showing the 25 μm emission from the cloud is displayed in Figure 1. The region shown is the same as that surveyed for molecular outflows in the cloud by Margulis and Lada (1986). As can be seen, the morphology of 25 μm emission in the region is very complex. Especially in the southern portion of the cloud the far-infrared emission is extended and many bright sources seem to overlap. As a result of this confusion, which in fact is even more acute at 60 and 100 μm, it was difficult to identify more than a handful of discrete sources from the co-added intensity maps alone. Therefore, additional maps of emission in the four *IRAS* bands were constructed from the four co-added maps. These additional maps were constructed by passing the co-added maps through a spatial filter which suppressed extended emission but passed emission from discrete sources. The details of this filtering procedure are described in Kleinmann *et al.* (1986). An example of such a map showing the filtered 25 μm emission from the cloud is shown in Figure 2. In the filtered maps many more sources were clearly defined and were, in fact, easy to identify. In general, sources with flux densities greater than 6 times the rms noise in both the filtered 25 μm maps and either the 25 μm unfiltered, 12 μm filtered, or 60 μm filtered maps were considered both here and in the original survey (Margulis and Lada 1986). The 6 σ detection limits (determined from the unfiltered maps) in the four *IRAS* bands are 0.24, 0.40, 0.60, and 5.1 Jy at 12, 25, 60, and 100 μm. In all, 30 sources were identified using these selection criteria. Their positions are noted in Figures 1 and 2.

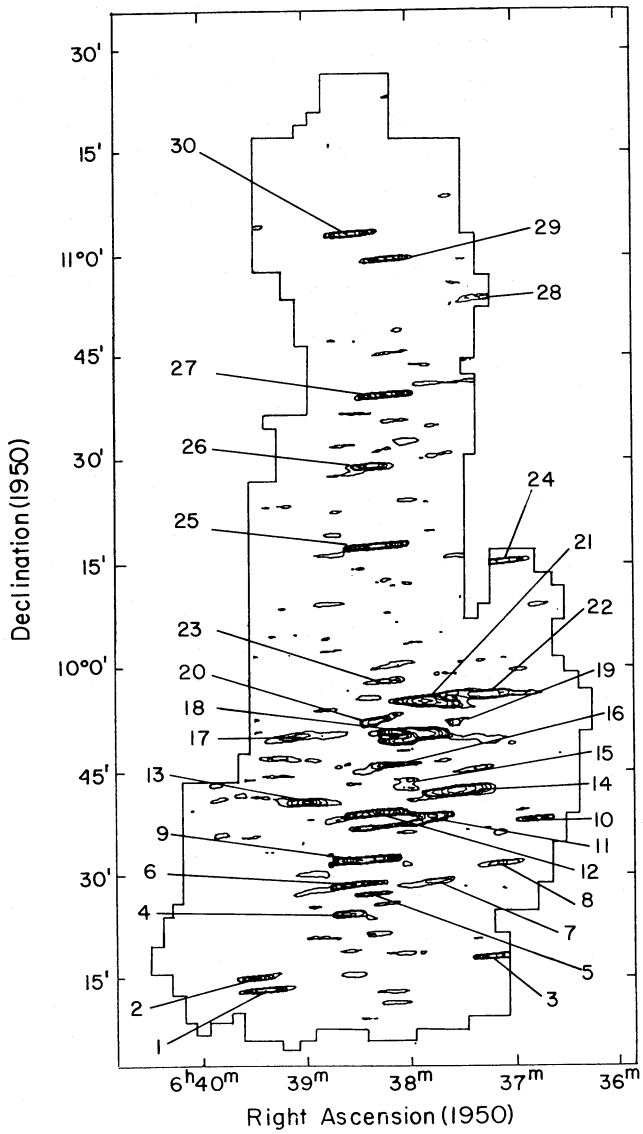

FIG. 2.—Same as Fig. 1 except that the emission at 25 μm has been passed through the point source filter discussed in the text. Contour levels are at 3.0, 6.0, 9.0, 12.0, 15.0, 20.0, 28.3, 40.0, 56.6, 80.0, 113.1, 160.0, 226.3, 320.0, 452.5, 639.9, 905.0, 1279.8, 1810.0, 2559.6, and 3619.9 times a base level of 0.042 Jy.

© American Astronomical Society • Provided by the NASA Astrophysics Data System

1989ApJ...345..906M

Although our selection criteria apppear somewhat conservative, our survey is by no means complete everywhere in the cloud. In a few regions located in the southern portion of the cloud the presence of extended far-infrared emission and source confusion resulting from the relatively low resolution of the *IRAS* observations have compromised our ability to identify discrete sources at low flux levels. In particular, faint sources situated very near bright, discrete sources in the cloud (which *were* identified) may have been passed over due to confusion. Thus for a small fraction of the area surveyed the detection limits in the four *IRAS* bands may be much higher than the 6 σ value quoted above. We estimate that, mostly due to the relatively large size of the *IRAS* beam at 25 μm, emission from bright, discrete 25 μm sources in the cloud occupies only about 3.4% of the surveyed area. Thus for 96.6% of the surveyed region the detection limits for our survey are the 6 σ limits given above, while for the remaining 3.4% of the region the detection limits may be considerably worse, in some cases as high as a few thousand sigma (for example, in places very near our source 9).

It is difficult to accurately estimate the overall completeness of our survey. This is because the presence of the NGC 2264 cluster in the southern portion of the complex suggests that the source density in the region (where almost all of the very bright *IRAS* sources are situated) may be considerably greater than in other areas of the molecular cloud. However, we can crudely determine a lower limit to our completeness by assuming that the surface density of *IRAS* sources is comparable to the surface density of bright ($m_v \leq 16$ mag) Hα sources in this region (Herbig 1954). With this assumption we expect that as many as seven far-infrared emitting sources could be located near enough to a very bright *IRAS* source to have escaped detection in our survey. If true, we have detected only about 80% of the far-infrared sources in the cloud. Thus we estimate that we have detected 80%–97% of all the sources in the surveyed portion of the cloud whose emitted flux densities at 25 μm and either 12 μm or 60 μm are equal to or exceed the limits quoted above.

Flux densities were obtained for the 30 identified sources from plots of intensity versus position made for each source along the *IRAS* in-scan direction in the unfiltered, co-added maps. An example of such a plot is shown in Figure 3. The in-scan direction, or the direction along which resolution on the sky was highest in the *IRAS* data, was very nearly parallel to lines of constant right ascension in the portion of the sky including the Mon OB1 molecular cloud. Thus these plots were made along lines running very nearly north-south. Flux densities were calculated from these plots by integrating the intensity over position using an appropriate baseline (fitted by eye), and by assuming that all of the sources were unresolved in the cross-scan direction (perpendicular to the in-scan direction). The brightest source in the region, Allen's infrared source (Allen 1972), was used as a calibrator. Flux densities for the calibrator were obtained by using the standard *IRAS* point source extractor on the co-added maps. The details of the extraction procedure can be found in Kleinmann *et al.* (1986). The resulting flux densities for Allen's source, our source 9 (990 and 1600 Jy at 60 μm and 100 μm, respectively), agree well with previous measurements made by Harvey, Campbell, and Hoffmann (1977; 980 and 1645 Jy at 53 and 100 μm) and with flux densities in the *IRAS* Point Source Catalog. In general, because essentially all of the sources had sizes in the in-scan direction less than the cross-scan resolution (source sizes will

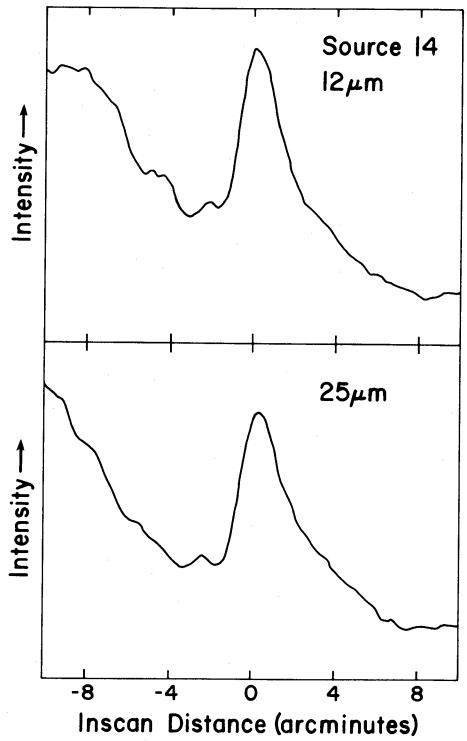

FIG. 3.—Plots of intensity vs. position of the 12 μm and 25 μm emission for a strip running along the in-scan direction through source 14.

be discussed in detail later in this paper), and because Allen's infrared source is a very strong, nearly unresolved source, we expect that for strong, isolated sources this procedure produced observed flux densities accurate to 15%. However, for weak sources in confused regions the uncertainties in the quoted flux densities are larger. This is especially true at 60 μm and 100 μm, bands at which *IRAS* observations were made with poor resolution for the purposes of this study. In the worst cases, we estimate that the observed flux densities may be in error by as much as 40% or possibly even more, the primary cause being source confusion.

Color corrections were applied to all of the observed flux densities except those of sources 16, 23, and 30 and the 100 μm flux densities of sources 21 and 26. Sources 21, 26, and 30 have energy distributions so steep that no accurate color correction could be made. For sources 16 and 23 only 12 μm flux densities were obtained so no color information was available. For the rest of the sources the 12 μm color correction was made using the correction obtained from the ratio of observed flux densities in the 12 μm and 25 μm bands, the 25 μm color correction was made using the average of the corrections obtained from the ratios of flux densities in the 12 μm and 25 μm bands and the 25 μm and 60 μm bands, the 60 μm color correction was made using the corrections obtained from the ratios of flux densities in the 25 μm and 60 μm bands and 60 μm and 100 μm bands, and the 100 μm color correction was made using the corrections obtained from the observed ratio of flux densities in the 60 μm and 100 μm bands. The appropriate color corrections as a function of color temperature are listed in Beichman *et al.* (1985). In all but a few cases the corrections were not more than 20% of the raw flux densities. In fact, in most cases the corrections were not more than 10%.

Flux densities in the four *IRAS* bands of the far-infrared

© American Astronomical Society • Provided by the NASA Astrophysics Data System

1989ApJ...345..906M

TABLE 1

FLUXES OF FAR-INFRARED DISCRETE SOURCES

Source (1)	α_{1950} (2)	δ_{1950} (3)	F_ν(12 μm) (Jy) (4)	F_ν(25 μm) (Jy) (5)	F_ν(60 μm) (Jy) (6)	F_ν(100 μm) (Jy) (7)
1.....	$6^h39^m22^s$	9°13′15″	0.2	0.9	13.	15.
2.....	6 39 28	9 15 00	0.3	0.8	2.8	8.0
3.....	6 37 08	9 18 29	2.5	0.6		
4.....	6 38 38	9 24 15				
5.....	6 38 25	9 27 30	0.3	0.4		
6.....	6 38 28	9 29 00	2.5	1.0		
7.....	6 37 45	9 29 30	0.7	1.2	3.7	
8.....	6 37 06	9 31 59	0.8	0.3		
9.....	6 38 26	9 32 30	160	300	990	1600
10.....	6 36 50	9 38 14	0.3	0.8	4.7	
11.....	6 37 48	9 38 30	4.9	6.2	13.	
12.....	6 38 18	9 39 04	8.3	10.	210	600
13.....	6 38 59	9 40 30	1.4	1.6	6.7	20.
14.....	6 37 33	9 42 29	7.0	6.9	24.	83.
15.....	6 38 00	9 43 45	0.7	1.0		
16.....	6 38 09	9 46 00	(1.1)			
17.....	6 39 04	9 50 00	1.2	1.7	8.8	16.
18.....	6 37 51	9 50 15	53.	65.	730	1100
19.....	6 37 36	9 51 59	0.2	0.6		
20.....	6 38 18	9 52 00	13.	9.8	140	450
21.....	6 37 51	9 55 00	16.	12.	100	(990)
22.....	6 37 14	9 55 43	8.1	13.	82.	280
23.....	6 38 09	9 58 00	(0.3)			
24.....	6 37 29	10 16 44	...	0.4	2.2	
25.....	6 38 17	10 18 10	3.6	8.5	73.	150
26.....	6 38 20	10 29 30	1.4	1.8	10.	(88.)
27.....	6 38 13	10 39 45	0.5	3.2	66.	150
28.....	6 37 13	10 53 59	0.4	0.6	2.8	8.3
29.....	6 38 09	10 59 30	0.6	1.1	1.8	
30.....	6 38 33	11 03 01	(10.)	(1.9)	(0.3)	

NOTE.—No color corrections have been applied to entries in parentheses.

sources identified are presented in columns (4) through (7) of Table 1 along with source names (col. [1]) and positions (cols. [2] and [3]). Except where noted, color corrections have been applied to all flux densities. Because many sources were weak and in regions where the morphology of far-infrared emission was complex, a flux density in each band for each source could not always be obtained, and the corresponding entries have been left blank. For source 4, in fact, no flux densities could be obtained. Although this source meets the selection criteria it is possible that it has been erroneously identified. In any case, it is clearly at the limit of detection.

In Table 2 source names, *IRAS* luminosities, 12 to 25 μm, 25 to 60 μm, and 60 to 100 μm color temperatures, and source spectral indices are presented. *IRAS* luminosities were calculated using the following equation:

$$L(L_0) = 60.1 L_0 \text{ Jy}^{-1} \text{ μm} \times \left[\frac{F_{\nu 12}}{(12 \text{ μm})^2} (18.5 \text{ μm} - 8.75 \text{ μm}) + \frac{F_{\nu 25}}{(25 \text{ μm})^2} 42.5 \text{ μm} - 18.5 \text{ μm}) + \frac{F_{\nu 60}}{(60 \text{ μm})^2} (80 \text{ μm} - 42.5 \text{ μm}) + \frac{F_{\nu 100}}{(100 \text{ μm})^2} (119.67 \text{ μm} - 80 \text{ μm}) \right], \quad (1)$$

where all the flux densities are in janskys. The color temperatures of the sources were derived from the color-corrected flux density ratios of the designated bands. Finally, the spectral indices were calculated using:

$$\text{Spectral Index} = \frac{\log \lambda_1 F_{\lambda_1} - \log \lambda_2 F_{\lambda_2}}{\log \lambda_1 - \log \lambda_2}, \quad (2)$$

with λ_1 and λ_2 equal to the most blueward and redward *IRAS* wavelengths at which flux densities could be obtained for each source (see Lada 1987). The values for λ_1 and λ_2 for each source are given in the column labeled "Bands" in Table 2. The values of $\lambda_1 F_{\lambda_1}$ and $\lambda_2 F_{\lambda_2}$ for each source were calculated from the data in Table 1.

Presented in Table 3 are the half-power diameters in the in-scan direction of each of the sources in each of the four *IRAS* bands. These sizes have been corrected for the in-scan size of the *IRAS* beam by assuming that both the in-scan beam profile and the source profiles are Gaussian in shape. The sizes of point sources in the in-scan direction have been entered in the table as zeroes. Dashes have been entered in the table in the cases where, due to confusion, no source size could be determined. Only a few of the sources identified in the Mon OB1 cloud are point sources. For example, at 12 μm many have half-power diameters in the in-scan direction greater than 2′ (see Table 3 and the sample source profile in Fig. 3) and corresponding radii (at 800 pc, the distance to the Mon OB1 cloud) greater than about 0.23 pc. In fact, as can be seen from Table 3 many sources are extended at longer wavelengths as well. These large source sizes cannot be easily explained by standard models of dust grain heating by starlight. The most likely

© American Astronomical Society • Provided by the NASA Astrophysics Data System

1989ApJ...345..906M

TABLE 2

LUMINOSITIES, COLOR TEMPERATURES, AND SPECTRAL INDICES OF DISCRETE SOURCES

Source (1)	Luminosity $L_\odot$ (2)	T(12/25) (K) (3)	T(25/60) (K) (4)	T(60/100) (K) (5)	Spectral Index (6)	Bands (7)
1.....	15.	180	65	57	+1.0	12–100
2.....	6.7	230	93	37	+0.5	12–100
3.....	11.	7300	...	...	−2.9	12–25
4.....						
5.....	2.0	290	...	...	−0.5	12–25
6.....	12.	790	...	...	−2.2	12–25
7.....	7.7	270	96	...	0.0	12–60
8.....	3.8	790	...	...	−2.2	12–25
9.....	2300	260	95	48	+0.1	12–100
10.....	5.7	210	79	...	+0.8	12–60
11.....	42.	310	110	...	−0.4	12–60
12.....	330	320	60	35	+1.0	12–100
13.....	18.	330	88	36	+0.3	12–100
14.....	79.	360	94	<35	+0.2	12–100
15.....	5.0	290	...	...	−0.5	12–25
16.....	(4.2)					
17.....	18.	300	82	43	+0.3	12–100
18.....	1100	310	68	50	+0.4	12–100
19.....	2.2	200	...	...	+0.7	12–25
20.....	270	430	65	35	+0.7	12–100
21.....	(390)	430	74	(<35)	(+0.9)	12–100
22.....	180	270	80	<35	+0.7	12–100
23.....	(1.3)					
24.....	2.2	...	79	...	+1.1	25–60
25.....	110	230	73	42	+0.7	12–100
26.....	(37.)	310	82	(<35)	(+1.0)	12–100
27.....	87.	160	60	39	+1.7	12–100
28.....	6.7	270	87	35	+0.5	12–100
29.....	6.1	250	120	...	−0.3	12–60
30.....	(45.)	(>10^4)	(>10^4)	...	(−3.3)	12–60

NOTE.—Color corrections have not been applied to some of the flux densities used to calculate the entries in parentheses.

explanation for the extended emission is that many of the sources identified herein are multiple and partially resolved by the *IRAS* beam. In fact, in many cases the source profiles actually exhibit structure in the in-scan direction suggestive of partially resolved components. We note that this no doubt introduces uncertainty and confusion in interpreting the derived spectral indices and flux densities of sources identified herein. Unfortunately, we found that it was not possible to reliably break up the extended source profiles into their constituent components. This is because (1) in many cases different numbers of components showed up in different bands for individual sources, (2) in many cases profile shapes were so complicated that it was not clear how many components contributed to emission for a source in an individual band, and (3) in some cases wings appeared on source profiles and it was not clear whether to include these as separate components. As a result, without higher resolution studies it is not possible to obtain better estimates of our derived spectral indices and flux densities. Sizes marked with an "m" in Table 3 denote extended sources whose intensity profiles showed evidence of multiple components.

Also presented in Table 3 are possible optical counterparts to the far-infrared point sources. In order to search for such counterparts the SAO catalog of bright stars (1966), the list of stars in Walker's (1956) classic study of the open cluster NGC 2264, and the list of Hα sources in Herbig's (1954) study of the cluster were searched in order to find optically visible stars coincident on the sky with the far-infrared sources identified toward the Mon OB1 cloud. An optical source was considered coincident if it lay within the half-power contour of a discrete *IRAS* source. In total 13 *IRAS* sources were found to have possible optical counterparts. In the northern portion of the cloud source 30 was found to have a bright optical counterpart listed in the SAO catalog. Source 30 is, in fact, HD 47886 (SAO 095997), a star of spectral type M1 III with an apparent visual magnitude of 6.1. At a distance of about 200 pc, this star is a foreground giant. In the southern portion of the cloud a second source could be identified with a bright optical counterpart. Source 3 is a foreground giant of spectral type M6 (Iijima and Ishida 1978).

Although it should also have been just possible to detect 12 μm emission from the O star in NGC 2264 (HD 47839), we find no evidence for a 12 μm point source at its position. Since the expected flux density for the O star at 12 μm is not large and the star is in a portion of the sky dominated by confusion in all four *IRAS* bands, we do not find our lack of a detection to be particularly surprising. Longward of 12 μm the expected flux density from the O star falls lower than the *IRAS* detection limits quoted in this paper.

Other optically bright members of NGC 2264 were too dim to be seen in the far-infrared. In Walker's original study of the cluster it was shown that stars with spectral types earlier than A0 lie on the main sequence while stars with spectral types from F0 to A0 lie in a band 2 mag brighter than the main sequence. Using standard values of the effective temperatures and sizes of main-sequence stars (Allen 1973) and using a distance to the cluster of 800 pc (Walker 1956), it can be shown that even a main-sequence cluster member with a spectral type

© American Astronomical Society • Provided by the NASA Astrophysics Data System

1989ApJ...345..906M

TABLE 3

SIZES AND OPTICAL COUNTERPARTS OF FAR-INFRARED DISCRETE SOURCES

Source	Size 12 arcmin	Size 25 arcmin	Size 60 arcmin	Size 100 arcmin	Coincident Optical Sources[a]
1.....	0	0	0	0	
2.....	0.8	0	0		
3.....	0	0	...	...	II30
4.....					
5.....	0	0	0	0	LHα49
6.....	0	0	...	...	LHα59, LHα61, LHα62
7.....	2.4 m	2.7 m	2.4		
8.....	0	0			
9.....	0	0	0	0	
10.....	0	0	2.1 m		
11.....	2.1 m	1.5 m	0		LHα18
12.....	0	0.9	0	0	LHα53
13.....	1.6 m	1.3 m	0	0	
14.....	2.3 m	2.2 m	2.0	0	
15.....	0.9	2.0 m	...	...	LHα23
16.....	0.9	...	...	...	LHα33
17.....	3.3 m	1.8 m	2.0	0	
18.....	3.6 m	3.1 m	3.7	4.8	LHα25
19.....	0	1.3 m			
20.....	4.1 m	3.7 m	4.3 m	4.2	LHα51
21.....	1.6	1.7	1.9	4.0 m	LHα19
22.....	3.3 m	4.1 m	4.5 m	4.5	
23.....	0.8	...	...	...	LHα31
24.....	...	1.2 m	0		
25.....	0.9 m	0	0	0	
26.....	1.4 m	1.4 m	2.4	...	LHα52
27.....	1.6	0	0	0	
28.....	1.3 m	0.9 m	2.2	0	
29.....	0	0	0		
30.....	0	0	0	...	HD 47886

[a] LHα = Herbig 1954; HD = Cannon and Pickering 1918; II = Iijima and Ishida 1978.

of B0 would not have been detected by *IRAS*. Therefore, even the stars in the cluster with the next earliest types after the O star should not have been detected. In fact, of the four B2 and B3 stars noted in Walker's study three have no far-infrared sources near them and the fourth has a nearby source with very cold color temperatures. As a result none of these stars might be physically associated with *IRAS* sources. The F0 to A0 stars as well, and five yellow giants found in the cluster by Walker, were also too dim to be detected in the far-infrared. In a similar way it can be shown that the 12 μm and 25 μm flux densities from these stars are at least an order of magnitude dimmer than the detection limits stated in this paper.

While no optically bright star in the cluster could be seen by *IRAS*, it is still possible that some of the optically dimmer stars in the cluster might have been detected in the far-infrared. In Walker's (1956) and Herbig's (1954) studies of the cluster it was noted that many of the redder, dimmer stars were variable in brightness and sources of Hα emission. These stars were identified as T Tauri stars. Since then it has been shown that many of these stars have strong infrared excesses at 2.2 μm (Warner, Strom, and Strom 1977), and it is likely that many are considerably brighter than blackbodies longward of 2.2 μm as well. As a result, a number of stars considered by Walker and Herbig might be associated with the far-infrared sources discussed here. It has been noted that stars of this type have spectral energy distributions which typically fall toward long wavelengths (e.g., $\lambda \geq 12$ μm) much less steeply than blackbodies (Rucinski 1985). In fact the typical spectral index for such stars (calculated from *IRAS* flux densities in Rucinski [1985] in a similar manner to those in Table 2) is −0.55. Using UY Aur, a T Tauri star with a spectral index from 12 μm to 60 μm of −0.6 (Rucinski 1985), as a typical star of this type, we estimate that in the absence of significant foreground extinction a T Tauri star in the cluster bright enough to be detected by *IRAS* would have an apparent visual magnitude brighter than about 16 (calculated from a rough *V* magnitude for UY Aur taken from Rydgren *et al.* 1985).

In the direction of the Mon OB1 cloud 49 Hα sources with *V* magnitudes brighter than 16 have been identified by Walker and Herbig. They are LHα3, LHα4, LHα10, LHα12, LHα13, LHα17, LHα18, LHα19, LHα20, LHα21, LHα22, LHα23, LHα25, LHα26, LHα27, LHα29, LHα30, LHα31, LHα33, LHα34, LHα35, LHα41, LHα43, LHα47, LHα48, LHα49, LHα51, LHα52, LHα53, LHα54, LHα59, LHα60, LHα61, LHα62, LHα65, LHα66, LHα68, LHα70, LHα71, LHα72, LHα73, LHα74, LHα75, LHα76, LHα77, LHα79, LHα82, LHα83, and LHα84. Of these as many as 11 might be associated with *IRAS* sources identified herein; two (LHα33 and LHα31) may be the optical counterparts of *IRAS* sources with only measured 12 μm flux densities (sources 16 and 23), one of three (LHα59, 61, or 62) might be the optical counterpart of *IRAS* source 6, a source with a negative spectral index, three (LHα49, 18, and 23) may be the optical counterparts of other *IRAS* sources with negative spectral indices (5, 11, and 15), and five (LHα53, 25, 51, 19, and 52) might be associated with *IRAS* sources with positive spectral indices (12, 18, 20, 21, and 26). However, 38 Hα stars with bright *V* magnitudes have no *IRAS* counterparts identified herein. It is possible either that this lack of identification is due to the confused morphology of the *IRAS* emission in the vicinity of the cluster/association

© American Astronomical Society • Provided by the NASA Astrophysics Data System

1989ApJ...345..906M

NGC 2264/Mon OB1 or that many of the Hα stars listed by Walker and Herbig have spectral energy distributions in the mid- and far-infrared more steeply falling than UY Aur's. In support of the latter possibility we note that if we relax the selection criteria stated earlier in this paper then as many as six more (LHα4, LHα13, LHα30, LHα43, LHα76, and LHα83) of the Hα stars identified by Walker may have *IRAS* counterparts at 12 μm. In any case either possibility would make many of the Hα stars impossible to detect using *IRAS* data alone.

Two *IRAS* sources with negative spectral indices (sources 8 and 29) have not been identified as Hα stars. Each of these sources do have optical sources near them, however (as can be seen from the POSS red plate of the region), and it is possible that these sources are Hα stars.

As can be seen less than half of the sources identified in the far-infrared have possible optical counterparts. In fact, we have in total listed only 13 sources with possible counterparts in Table 3. This is not surprising since, by selecting sources on the basis of far-infrared brightness, we have chosen a sample biased toward young, deeply embedded objects hidden by dust at *U*, *B*, and *V*. As we shall discuss these sources are likely to be very young, in fact, in a pre–Tauri stage of evolution.

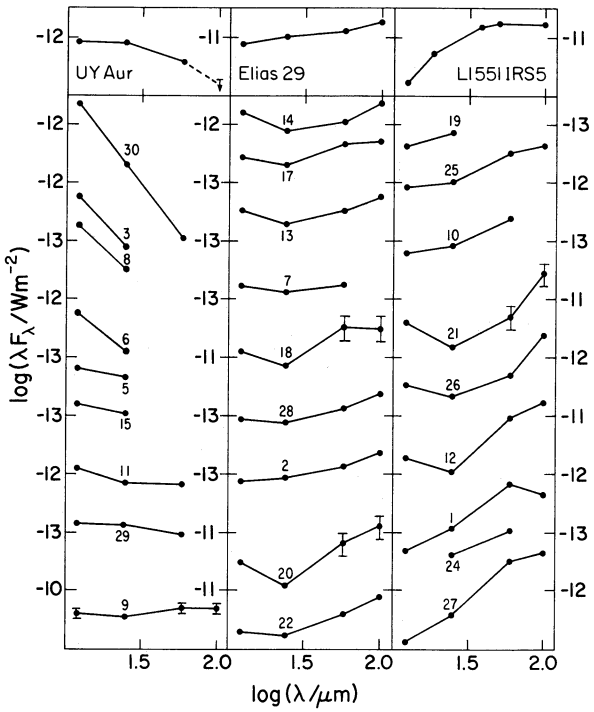

FIG. 4.—Spectral energy distributions of far-infrared point sources identified in the direction of the Mon OB1 cloud. The distributions have been arranged in order of increasing spectral index from the top left to the bottom right. The positive number next to each distribution is the name of the source. Nine spectral energy distributions have been included in each column of the figure. Nine corresponding tickmarks on the vertical axes of the figure have been included for scale. In general, the value next to the tickmark at the top corresponds to the top most spectral energy distribution, the value second from the top corresponds to the second energy distribution from the top, and so on. For all sources the distance between the tickmarks is one order of magnitude in λF_λ. Representative 15% error bars are included on the 12 μm, 60 μm, and 100 μm data points of source 9, and representative 40% error bars have been included on the 60 μm and 100 μm data points of sources 18, 20, and 21. Also shown in separate boxes at the top of the figure are the far-infrared spectral energy distributions of UY Aur, Elias 29, and L1551 IRS 5. These spectral energy distributions are shown for the purpose of comparison and are displayed on similar scales to the distributions in the bottom half of the figure.

In addition to the tables, the far-infrared data are also presented as four band spectral energy distributions in Figure 4. In the figure source spectral energy distributions are displayed in order of increasing spectral index from top to bottom and left to right. In addition the far-infrared spectral energy distributions of UY Aur (Rucinski 1985), Elias 29 (Young, Lada, and Wilking 1986), and L1551 IRS 5 (Cohen and Schwartz 1983; Cohen *et al.* 1984) are also shown for reference. As can be seen there is a smooth progression from steeply falling sources (*top left*) through flat sources to steeply rising sources (*bottom right*) in the figure.

Even though we have characterized each source in our survey by a single-valued (i.e., power law) spectral index (i.e., eq. [2] and col. (6) in Table 2), it is clear from Figure 4 that the *IRAS* energy distributions of many sources are not adequately described by a single-valued slope. For example, we have derived (relatively large) positive spectral indices for sources 12, 18, 20, and 21 between 12 μm and 100 μm. However, if we had considered only the flux densities at 12 μm and 25 μm, the spectral indices derived (eq. [2]) for the same objects would all have been negative! It is likely that the observed structure in the energy distributions, which result in multivalued, wavelength-dependent spectral indices for these *IRAS* sources, is due to the superposition of at least two infrared sources with differing spectral indices within a single *IRAS* beam. As pointed out in Table 3, sources 12, 18, 20, and 21 are all extended and sources 18, 20, and 21 exhibit evidence for multiple components in their in-scan intensity profiles. Moreover, sources 12, 18, 20, and 21 are positionally coincident with Hα stars, and it is possible that these stars contribute most of the emission at 12 μm. On the other hand, since such stars are usually characterized by energy distributions which decrease with increasing wavelength, an additional colder and more heavily obscured source (or sources) is probably required to explain the emission at longer wavelengths.

III. DISCUSSION

a) The Natures of the Young Stellar Objects in the Monoceros OB1 Complex

Many types of young stellar objects can be found in the Mon OB1 cloud and accompanying association (NGC 2264/Mon OB1). As can be seen from the spectral energy distributions displayed in Figure 4, *IRAS* sources with spectral energy distributions falling, flat, and rising toward the far-infrared have been identified. In addition, in Herbig's (1954) and Walker's (1956) studies and numerous subsequent studies of the association, main-sequence stars, stars lying above and to the right of the main sequence, and stars showing brightness variability, Hα emission, and near-infrared excesses have been identified. Together these sources constitute a large sample containing examples of every known type of young stellar object.

In order to investigate the natures of the many young stellar objects identified in the Mon OB1 cloud and accompanying association it is worthwhile to classify them according to their properties. Recently from observations of the shapes of the spectral energy distributions of young stellar objects embedded in the Ophiuchus molecular cloud core (Lada and Wilking 1984; Lada 1987), it has been shown that almost all such objects can be grouped into three broad but well-defined classes numbered I through III. Class I sources are objects with spectral energy distributions much wider than single blackbodies and positive spectral indices in the near- and mid-

© American Astronomical Society • Provided by the NASA Astrophysics Data System

1989ApJ...345..906M

infrared (in the $\log \lambda F_\lambda$ versus $\log \lambda$ plane). Such energy distributions are characteristic of sources deeply enshrouded by dust. Objects with spectral energy distributions like those of T Tauri stars comprise the sources in class II. These objects also have spectral energy distributions wider than single blackbodies but have negative spectral indices in the mid- and far-infrared. Objects with spectral energy distributions like those of reddened photospheres comprise those in class III. Like sources in class II these objects are characterized by negative spectral indices in the infrared, but have spectral energy distributions with widths comparable to those of blackbodies.

Of the 30 *IRAS* sources which we have identified in the direction of the Mon OB1 cloud, probably only two are clearly class III objects. These objects are sources 3 and 30 in Table 1, the M stars. Since the M stars are not physically associated with the Mon OB1 cloud, they will not be considered in most of the discussion which follows. We note in contrast, however, that many optically visible class III objects have been identified in the direction of the Mon OB1 cloud in the past. In Walker's (1956) study of the stellar association, for example, many stars lying on the main sequence and lying just above and to the right of the main sequence were identified. These objects had the *UBV* colors of reddened photospheres. They did not, however, exhibit brightness variability or Hα emission lines, and a subsequent study (Warner, Strom, and Strom 1977) has shown that few if any exhibit infrared excesses. As a result these objects probably all fit into class III. In fact, a proper motion survey by Vasilevskis, Sanders, and Balz (1965) has shown that $\frac{2}{3}$ to $\frac{3}{4}$ of the optically visible sources in the association are likely to fall into class III. None of these objects were detected by *IRAS*.

IRAS did, however, detect a number of class II objects in the Mon OB1 cloud. A study of *IRAS* emission from well-known T Tauri stars (Rucinski 1985) has shown that the *IRAS* spectral indices of these sources (calculated in the same way as those in Table 2) average around −0.55 and only very rarely are greater than zero. Moreover, their energy distributions are often well described by a single-valued spectral index at infrared wavelengths (e.g., Adams, Lada, and Shu 1988). As a result it seems likely that of the 30 sources identified herein any source with an *IRAS* spectral index less than about zero (other than the M stars) is likely to be a class II object. This places sources 5, 6, 8, 11, 15, and 29 into class II. In addition, it seems likely that sources 16 and 23, objects detected only at 12 μm but coincident with Hα stars LHα33 and 31, are also class II sources. Note that many of these sources have spectral energy distributions similar to that of UY Aur, a typical T Tauri star (see Fig. 4). In Walker's (1956) study of Mon OB1, as well, 79 optically visible stars were found to exhibit brightness variability and/or Hα emission and many of these stars at the time were classified as T Tauri stars. In addition, all of the stars of this type subsequently observed in the infrared show strong excesses at 2.2 μm (Warner, Strom, and Strom 1977). With infrared excesses in the near-infrared it is not surprising that some of these class II sources are bright in the mid- and far-infrared as well. In addition to LHα33 and LHα31 (sources 16 and 23) four additional *IRAS* sources with negative spectral indices identified herein (sources 5, 6, 11, and 15) may also have optically visible T Tauri star counterparts. However, as mentioned earlier, most of the Hα stars identified by Walker (1956) and Herbig (1954) are not bright enough in the infrared to be detected by *IRAS*. In fact, at least 38 Hα stars with *V* magnitudes (and thus luminosities) about the same as the *IRAS* class II sources discussed here were not identified in the far-infrared.

In addition to objects in classes III and II, class I objects have also been detected by *IRAS* toward the Mon OB1 cloud. In fact, the majority of objects detected by *IRAS* fall into class I. It is clear that many of the 30 objects identified have spectral indices greater than about zero, meaning that they have more steeply rising far-infrared energy distributions and colder color temperatures than T Tauri stars. In addition, the spectral energy distributions of these objects are much wider than blackbodies. In fact, among these (source 9) is the well-known Allen's protostellar object (Allen 1972; Harvey *et al.*; Wynn-Williams 1982) and an object (source 12) observed previously at 70 and 130 μm by Sargent *et al.* (1984, source NGC 2264 FIR), at 40 to 160 μm by Cohen, Harvey, and Schwartz (1985), and thought to be deeply embedded in natal material in the Mon OB1 molecular cloud. These facts suggest that many of the far-infrared sources identified are deeply embedded in natal material in the Mon OB1 cloud. As a result it seems likely that sources 1, 2, 7, 9, 10, 12, 13, 14, 17, 18, 19, 20, 21, 22, 25, 26, 27, and 28 all fit into class I and contain at least one component which is a heavily obscured young stellar object. Note that many of these sources have similar spectral energy distributions to Elias 29 or L1551 IRS 5, typical class I sources the spectral energy distributions of which are displayed in Figure 4.

Only five of 18 *IRAS* sources which we have classified as class I objects (i.e., 12, 18, 20, 21, and 26) are coincident with known, visible Hα stars. The facts that (1) the energy distributions of all these sources have negative spectral indices between 12 μm and 25 μm but positive indices longward of 25 μm, and (2) the *IRAS* emission at 12 μm is extended toward all sources except source 12, suggest that at least four of these sources are multiple (as discussed earlier) and that the objects responsible for the bulk of the far-infrared emission longward of 25 μm (and therefore the bulk of the observed source luminosity) are probably not currently known visible stars.

Finally, we note that two sources in the cloud could not be easily categorized. Source 4 was too weak for accurate flux densities to be obtained and neither 12 μm nor 100 μm flux densities could be obtained for source 24. As a result we leave them out of much of the discussion which follows.

In summary, 28 of the 30 *IRAS* sources could be fitted into the spectral classification system. Two sources fall into class III, eight sources fall into class II, and 18 sources fall into class I. The dividing line between classes III and II is about a spectral index of −2.5. The dividing line between classes II and I is about a spectral index of zero. In contrast to the results of previous studies of optical and near-infrared emission from the sources in the region, the majority of sources in the *IRAS*-selected sample are identified as class I objects.

We note, in addition, that many of the *IRAS* sources identified are located in the Mon OB1 cloud behind the Mon OB1 association. This suggests that star formation continues to go on behind the association in spite of the fact that literally hundreds of stars have already formed in the region (see, for example, the list of young stellar objects in Adams, Strom, and Strom 1983). Clearly, star formation in molecular clouds is a continuous and ongoing process lasting perhaps as long as the lifetime of the clouds themselves.

We display in Figure 5 the *IRAS* luminosity functions of the sources in classes I and II. Sources 16 and 23, probably class II *IRAS* sources, have been left out of the figure since their luminosities are based on flux densities measured at 12 μm only. As can be seen the brightest sources are clearly in class I. This is what is expected since, by definition, class I sources emit most

© American Astronomical Society • Provided by the NASA Astrophysics Data System

1989ApJ...345..906M

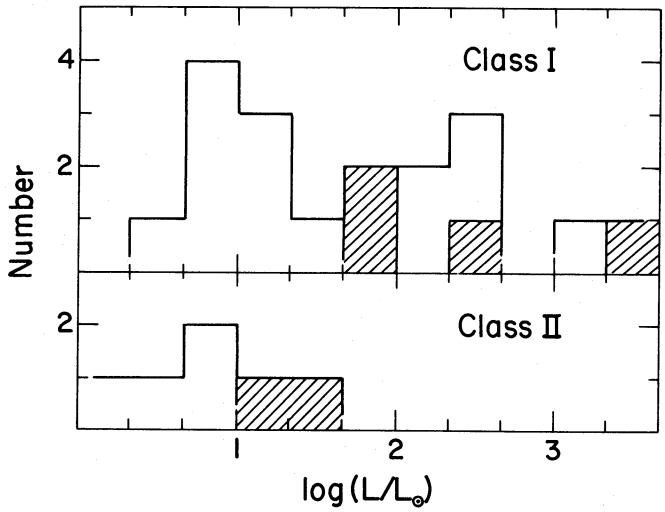

FIG. 5.—*IRAS* luminosity function of class I (*top*) and class II (*bottom*) sources identified toward the Monoceros OB1 molecular cloud. Hatchmarked regions in the figure denote sources associated with outflow candidates.

of their luminosity in the far-infrared (Lada 1987). Moreover, as a result we expect that their *IRAS* luminosities, quoted in this paper, are very nearly bolometric. In contrast, however, class II sources emit most of their luminosity in the near-infrared and optical, and will be selected against in an *IRAS*-based sample. The *IRAS* luminosities of these sources are much less than their true bolometric luminosities. Clearly it would be more meaningful and useful to make a comparison between the bolometric luminosities of sources in the two classes. In order to do so one must make a bolometric correction to the *IRAS* luminosities of the class II sources. We have attempted to do this. Using a composite spectral energy distribution of seven T Tauri stars presented in Adams, Lada, and Shu (1988) we have calculated the emergent luminosities of a typical T Tauri star in the *IRAS*, near-infrared, and optical wavelength regimes. From this we find that the bolometric luminosity for a typical class II source is roughly 6 times its *IRAS* luminosity. Making this correction to the histogram in Figure 5 amounts to sliding the *IRAS* luminosity function for class II sources a little more than two bins to the right. Note that even with this correction the most luminous sources are still in class I. In fact, if all potential class II sources with bolometric luminosities above about 5 $L_\odot$ are considered (eight class II *IRAS* sources and 38–43 Walker Hα sources with $V < 16$ but not clearly identified with *IRAS* sources), then only two of these sources (4%) have bolometric luminosites greater than about 60 $L_\odot$. In contrast nine out of 18 (50%) of the detected class I sources (all with luminosities above about 5 $L_\odot$) are more luminous than 60 $L_\odot$. These facts suggest that there is a true difference between the *bolometric* luminosity functions of class I and II sources in the Mon OB1 cloud. A similar luminosity segregation of class I and II sources has been observed in the Ophiuchus dark cloud (Wilking, Lada, and Young 1989).

The possibility that some of the brighter class I sources in the cloud may be multiple is unlikely to significantly affect the difference in the luminosity functions of the two classes. As discussed in § II of this paper, the large sizes and unusual spectral energy distributions of sources 18, 20, 21, and 22 suggest that these sources may be composed of two components, one which produces the bulk of the emission observed at 25 μm and longward and one which produces some of the emission observed at 12 μm. For each of sources 18, 20, 21, and 22 the long-wavelength component is clearly in class I and produces most of the *IRAS* emission from the source. Thus its luminosity should not be significantly different from the *IRAS* luminosity calculated for each source in total. Furthermore, since adjacent bins in Figure 5 represent over a factor of 2 difference in luminosity, even two components of similar luminosity would not occupy significantly different places from that of the multiple source they comprise in the luminosity function in Figure 5.

Our analysis of the *IRAS* energy distributions of *IRAS* sources in the NGC 2264 molecular cloud complex supports earlier contentions (Lada and Wilking 1984; Lada 1987; Adams, Lada, and Shu 1987) that the empirical sequence of source spectral classes I, II, and III represents a quasi-continuous sequence of differing stages of evolution in the formation and early development of stars. The physical basis for this contention is that the observed variation in spectral class is a direct result of a variation in the amount of circumstellar dust surrounding the various sources (Lada 1987). This is evident in the NGC 2264 data from the facts that (1) class I sources are most often completely obscured from view at optical wavelengths and radiate the bulk of their luminosity in the far-infrared, giving them enormous infrared excesses; (2) class II sources are mostly associated with optically visibile T Tauri stars, radiate the bulk of their luminosity in the optical and near-infrared, but at the same time display small to moderate infrared excesses; and (3) class III sources are bright in the optical and have energy distributions similar to those of normal stars displaying no infrared excess (and therefore no evidence for circumstellar dust). The empirical sequence from I to III is therefore a sequence in which progressively less circumstellar dust is associated with a young stellar object. This sequence was first noted for the embedded sources in the Ophiuchus dark cloud and was qualitatively interpreted as a sequence in which class I sources were the least evolved objects in the cloud due to their most intimate association with circumstellar material (Lada and Wilking 1984; Lada 1987). Successful modeling of class I energy distributions as the emergent intensity distributions of rotating, collapsing protostars (Adams and Shu 1986; Adams, Lada, and Shu 1987) provides strong support for such an interpretation. Moreover, class II sources have been successfully modeled as post-infall objects, that is, protostellar systems stripped of their relatively massive infalling envelopes (Adams, Lada, and Shu 1987).

In the context of such evolutionary scenarios our observations of a bolometric luminosity difference between class I and class II sources has (at least) two interesting and plausible interpretations. First, it is possible that class I and class II sources in the cloud are objects of similar (final) mass. The higher luminosity of class I sources is then the result of source evolution. Indeed, theoretical models of protostars (e.g., Stahler, Shu, and Taam 1980; Adams, Lada, and Shu 1987) suggest that objects which ultimately produce solar mass (and luminosity) main-sequence stars can attain relatively high luminosities (≈30–60 $L_\odot$, e.g., WL 16, Elias 29, and L1551 IRS 5) during their protostellar evolution. The source of this "additional" luminosity is the thermalization of gravitational potential energy at an accretion shock produced by the infall of circumstellar material onto an embryonic stellar core and its surrounding disk. Once the initial envelope of a protostar is dissipated, and the protostar becomes a class II object, the

© American Astronomical Society • Provided by the NASA Astrophysics Data System

1989ApJ...345..906M

source of this additional infall luminosity is removed. In this case our observations may provide an important additional piece of evidence implicating class I sources as protostellar in nature.

However, seven of the 18 class I sources we detected have luminosities of 100 $L_\odot$ or greater, which is higher than the typically predicted maximum luminosities of solar mass protostars ($\approx 60\ L_\odot$, Stahler, Shu, and Taam 1980; Adams, Lada, and Shu 1987). If a single object is responsible for producing the bulk of the *IRAS* emission from each of the sources, then the bright class I *IRAS* sources must be systematically more massive than the known class II objects in the region. Although no class II sources have been identified with luminosities this large, there are about 17 class III stars in the cluster with luminosities in excess of 100 $L_\odot$ (see the H-R diagram in Walker 1956). Since the evolutionary tracks on the H-R diagram are horizontal for stars with these luminosities (i.e., $M_* \geq 3\ M_\odot$), roughly 29% (7) of all stars with luminosities greater than 100 $L_\odot$ *ever* produced from this complex are presently class I sources deeply embedded in natal material! Walker (1956) pointed out that cluster members with spectral types earlier than A0 (i.e., $L_* \geq 100\ L_\odot$) were all on the ZAMS, giving a well-determined contraction (turn on) age of the cluster of almost 3×10^6 yr. If the rate of (massive) star formation were constant over this period, our data would suggest a duration of the class I phase of about 9×10^5 yr for stars with $L > 100\ L_\odot$. Since this is also comparable to the pre–main-sequence contraction times for such stars we might not expect to see many objects with class II energy distributions, since they will already have arrived on or very nearly on the main sequence by the time they have dissipated their infalling envelopes and circumstellar disks and become visible.

b) *Association with Molecular Outflows*

As stated above, both the identified *IRAS* and previously identified optical sources observed toward the Mon OB1 cloud can be categorized into three classes representing reddened photospheres of pre–main-sequence and main-sequence stars (class III), T Tauri stars (class II), and sources deeply embedded in natal material (class I). Since the portion of the Mon OB1 cloud over which these sources are situated has also been completely surveyed for the presence of molecular outflows (Margulis and Lada 1986; Margulis, Lada, and Snell 1988), it is now possible to compare the positions of these sources with those of the outflows, and investigate the nature of the young stellar objects that are typically associated with outflow. First, we note that while only 30 *IRAS* sources have been identified toward the cloud, over 600 optical sources have been identified (Herbig 1954; Walker 1956; and Adams, Strom, and Strom 1983), and many of these exhibit Hα emission and are likely to be young stellar objects. As a first step, then, toward identifying the type of source associated with molecular outflows, we first must investigate the question of whether *IRAS* sources, optically visible sources, or both are associated with outflows.

In order to decide this we consider individually the entire portion of the Mon OB1 cloud surveyed for outflows (Margulis, Lada, and Snell 1988) and *IRAS* sources, and a subset of this region which has been completely surveyed for molecular outflows (Margulis, Lada, and Snell 1988), *IRAS* sources, and optically visible young stellar objects (Herbig 1954; Walker 1956; Adams, Strom, and Strom 1983). The latter region is the union of regions a, b, c, and d denoted in Adams, Strom, and Strom (1983).

Over the entire portion of the Mon OB1 cloud surveyed for outflows and *IRAS* sources, nine suspected molecular outflows have been identified (labeled A through I in Margulis, Lada, and Snell 1988). If we say that any *IRAS* source which falls within 3.5 of the center of a suspected outflow (positions of outflow candidate centers and pictures of the outflow candidates along with positions of nearby *IRAS* sources are given in Margulis, Lada, and Snell 1988) is considered to be coincident with it, then we find that in this region six (candidates B, C, D, E, F, and H) of the nine suspected outflows have coincident *IRAS* sources. Outflow candidate B is coincident with *IRAS* sources 4, 5, and 6, of which 6 is closest to the candidate's center, outflow candidate C is coincident with *IRAS* sources 6 and 9, of which 9 is closest to the candidate's center, outflow candidate D is coincident with *IRAS* source 12, outflow candidate E is coincident with *IRAS* sources 11 and 14, of which 11 is closest to the candidate's center, outflow candidate F is coincident with *IRAS* source 14, and outflow candidate H is coincident with *IRAS* source 27. It is *extremely unlikely* that this high rate of coincidence has occurred by chance. The region surveyed for outflows and far-infrared sources was 5276 square arcminutes in size. Inside this region there are only 30 *IRAS* sources and nine outflow candidates. Monte Carlo simulations suggest that there is only a one in 505 chance that at least six of the suspected outflows might have coincident *IRAS* sources. As a result it seems likely that the *IRAS* sources and outflow candidates in the region are physically associated.

Over the smaller (625 square arcminute) region which has been completely surveyed for molecular outflows, *IRAS* sources, and optically visible young stellar objects there are five suspected molecular outflows (candidates B, C, D, E, and F, Margulis, Lada, and Snell 1988), 10 *IRAS* sources (sources 4, 5, 6, 7, 9, 11, 12, 14, 15, and 16), and 29 Hα sources with V magnitudes brighter than 16 (Herbig 1954; Walker 1956). Once again if we say that any *IRAS* or Hα source which falls within 3.5 of the center of a suspected outflow is coincident with it, then as noted above all five of the suspected outflows have coincident *IRAS* sources. In addition, four have coincident Hα sources. Outflow candidate B is coincident with Hα sources LHα59, 61, 62, 65, and 72 (Herbig 1954), outflow candidate C is coincident with Hα sources LHα43, 54, 59, 61, 62, 65, and 71, outflow candidate D is coincident with Hα sources LHα35, 47, and 53, and outflow candidate E is coincident with Hα sources LHα10 and 12. The probability that by chance one or more *IRAS* sources might be coincident with each outflow in the region is 1 in 86. On the other hand, the probability that by chance one or more of the bright Hα sources might be coincident with four of the five outflow candidates in the region is 4 in 5. As above it seems likely that *IRAS* sources and outflow candidates in the region are physically associated. From here forward we adopt this viewpoint and assume that the coincidence of bright Hα sources and suspected outflows in the region is due to chance superposition.

The *IRAS* sources associated with suspected outflows are indicated (by hatchmarks) in Figure 5. Four outflow sources (C, D, F, and H in Margulis, Lada, and Snell 1988) are found to be associated with class I *IRAS* sources and two (B and E) with class II sources. Moreover, the *IRAS* sources associated with outflows are among the most luminous examples of their spectral class. Indeed, if a bolometric correction is applied to the two class II objects associated with outflows, we find that six of the 11 luminous (i.e., $L_{\rm bol} > 50\ L_\odot$) *IRAS* sources in the cloud are associated with candidate molecular outflow sources.

© American Astronomical Society • Provided by the NASA Astrophysics Data System

1989ApJ...345..906M

Similar high detection rates for outflows associated with luminous infrared sources have been found before (Bally and Lada 1983; Snell *et al.* 1988). Our results could be interpreted to mean that either half the luminous *IRAS* sources in the cloud produce detectable molecular outflows, or that the outflow phase occupies roughly half the lifetime of a typical luminous *IRAS* source. In either case our observations clearly indicate that the molecular outflow phase lasts a significant fraction (50%–100%) of the lifetime of a luminous *IRAS* source and that the production of molecular outflows is a common consequence of the star-formation process for at least those stars which begin their evolution as luminous ($L \geq 50\ L_\odot$) *IRAS* sources. Indeed, even if we consider all our data and ignore the possible luminosity selection effects, then 22% of the class I sources and 30% of the class II *IRAS* sources have outflows, indicating that at least 20% of the lifetime of an *IRAS* source with $L > 5\ L_\odot$ is spent in the outflow phase! The fact that nine of the 11 *IRAS* sources with $L_{bol} > 50\ L_\odot$ are class I sources suggests that a luminous young stellar object spends less than 20% of its lifetime as a luminous class II source. Since the six *IRAS* sources associated with outflows all have bolometric luminosites greater than $50\ L_\odot$, our observations therefore suggest that the outflow phase occurs in the earliest stages of pre–main-sequence and protostellar evolution. From Figure 5 we see that four of the outflows are associated with class I sources while two are associated with class II objects which are the most luminous, and presumably the least evolved class II objects in the cloud. It is likely that outflow is initiated sometime during the class I phase and persists until early into the class II phase of evolution. This is consistent with suggestions that outflow is the agent which drives the evolution of a class I source to a class II source by removing the circumstellar envelope around a protostellar object (Lada 1987; Adams, Lada, and Shu 1987; Myers *et al.* 1988; Snell *et al.* 1988).

The lack of detectable molecular outflows around the lower luminosity ($L < 50\ L_\odot$) *IRAS* sources in the cloud could be due to either a real absence of such activity around these sources or observational selection. The original outflow survey (Margulis and Lada 1986) was capable of detecting flows with mechanical energies comparable to or greater than of L1551, which itself is driven by a relatively luminous ($L \approx 30\ L_\odot$) class I source. Therefore, since the mechanical energies of flows scale roughly with the luminosities of their driving sources (Bally and Lada 1983), we do not necessarily expect to have detected outflows around the lower luminosity objects in the cloud. Studies of outflows in other clouds suggest that lower energy outflows do indeed occur with the same frequency around lower luminosity ($L \leq 30\ L_\odot$) objects (Myers *et al.* 1988) as found here and elsewhere (Snell *et al.* 1988) for high-luminosity sources. However, more sensitive CO surveys of the *IRAS* sources are needed to determine if this is also the case for the Mon OB1 cloud. It is intriguing, in this context, that three possible molecular outflows were detected in the cloud but do not have obvious *IRAS* or optical driving sources (flows A, G, and I; Margulis, Lada, and Snell 1988). These flows are probably driven by sources with luminosities ($L_{bol} \leq 5\ L_\odot$) lower than our survey limit in this paper. Evidently, even low-luminosity young stellar objects are capable of occasionally producing relatively energetic molecular outflows.

Finally, it is also possible using the data presented herein to quantify our knowledge of the birthrate of outflow driving sources in the solar neighborhood. As just discussed 54% of young stellar objects more luminous than $50\ L_\odot$ in the Mon OB1 cloud have associated outflow candidates. If all of these candidates are, in fact, outflows then this suggests that at least 54% of all young stellar objects in the solar neighborhood more luminous than $50\ L_\odot$ must go through the outflow phase sometime during their early evolution. The birthrate of outflow sources in the solar neighborhood must therefore be at least 54% of that for main-sequence stars more luminous than $50\ L_\odot$ or 3×10^{-5} kpc^{-2} yr^{-1} (birthrate calculated from those in Ostriker, Richstone, and Thuan 1974). This value is about equal to the birthrate in the solar neighborhood of $4\ M_\odot$ stars, and suggests that the birthrate of outflow driving sources must be at least as high as that of late B stars. It should be noted that this birthrate is determined in a way completely independent from those in which outflow birthrates have been determined before (see, for example, Bally and Lada 1983; Lada 1985). In particular, no estimate of a typical outflow lifetime was used in deriving this value.

We note that the birthrate derived here is about 30 times less than that derived previously from the number of outflows found in the Mon OB1 cloud (10^{-3} kpc^{-2} yr^{-1}, Margulis, Lada, and Snell 1988). However, since the birthrate derived here is clearly a lower limit the difference between the two values may not be a problem. As a matter of fact, the birthrate derived here could easily be increased by an order of magnitude if one considers that the luminosity limit, $50\ L_\odot$, used in order to calculate it is the luminosity of a very young stellar object. Theoretical models of young stellar objects have shown that even solar mass stars may have luminosities around $50\ L_\odot$ during the earliest stages of their evolution (Stahler, Shu, and Taam 1980; Adams, Lada, and Shu 1987). Solar mass stars, of course, have a much higher birthrate than that used above. Thus if one could ascertain the ultimate main-sequence luminosity of a $50\ L_\odot$ young stellar object, then a more accurate and higher birthrate for outflow sources could be found. In fact, even if there was still a discrepancy after taking this into account the remaining difference between the birthrate derived here for *outflow driving sources* and that derived in Margulis, Lada, and Snell (1988) for *outflows themselves* could be explained if outflow sources go through multiple outflow bursts. Multiple outflow bursts are, in fact, a likely possibility. In spite of the fact that very young stellar objects are often associated with outflow (Bally and Lada 1983; Myers *et al.* 1988; Snell *et al.* 1988), the estimated lifetimes of very young stellar objects are thought to be longer than the dynamical timescales of flows themselves. This suggests that either the estimated lifetimes of these objects are greatly in error or that outflow driving sources do go through multiple episodes of outflow.

IV. CONCLUSIONS

We have presented detailed results of a survey of a large portion of the Monoceros OB1 molecular cloud for discrete far-infrared sources. The survey was performed using co-added maps at 12, 25, 60, and 100 μm made from the *IRAS* data base. The region surveyed was the same as that surveyed for molecular outflows in the Monoceros OB1 molecular cloud (Margulis and Lada 1986). Using somewhat conservative selection criteria 30 discrete *IRAS* sources were identified in the region. Of these about two-thirds were found to be extended relative to the *IRAS* beam, suggesting that many of the sources are likely to be the result of the superposition of two or more far-infrared–emitting objects. *IRAS* spectral energy distributions

© American Astronomical Society • Provided by the NASA Astrophysics Data System

1989ApJ...345..906M

were constructed for 27 of the 30 sources. Although many of the discrete far-infrared sources in the cloud may be multiple, we could fit most of them into a spectral classification system for young stellar objects based on the shapes of their spectral energy distributions. Eighteen *IRAS* sources were found to have class I energy distributions, characteristic of deeply embedded/protostellar objects. Eight *IRAS* sources were found to have class II energy distributions, typical of partially obscured T Tauri stars with circumstellar disks. Two *IRAS* sources had class III energy distributions, characteristic of normal stellar photospheres, and two *IRAS* sources could not be classified. The presence of many bright class I sources in the Mon OB1 cloud indicates that active star formation is still occurring in the complex which produced the visible cluster, NGC 2264. Our data are consistent with a roughly constant rate of star formation in this complex over the last 3×10^6 yr.

Far-infrared luminosities were calculated for each source by integrating under its *IRAS* spectral energy distribution. After making a bolometric correction we find that the bolometric luminosity functions for class I and class II sources in the Mon OB1 cloud are significantly different. In particular, of all class I and II sources more luminous than 5 $L_\odot$, 50% of class I sources are more luminous than 60 $L_\odot$ while only 4% of class II sources are. There are (at least) two possible explanations for this luminosity segregation. It is possible that class I and II sources in the cloud will ultimately evolve into stars of similar mass. In this case the excess luminosity of class I sources is probably due to the thermalization of gravitational potential energy at an accretion shock where material in an infalling circumstellar envelope collides with an embryonic stellar core and its associated disk. Class I sources are therefore surrounded by massive circumstellar envelopes while class II sources are not. This intepretation is consistent with models of early stellar evolution which suggest that the empirical sequence of classes I, II, and III is a sequence in which progressively less circumstellar dust is associated with a young stellar object. On the other hand, it is likely that the highest luminosity class I sources will ultimately evolve into higher mass stars than will the observed class II objects. In this case the lack of luminous class II sources is due to the fast evolution of high-mass stars in the H-R diagram; by the time a high-mass young stellar object has dispersed its circumstellar envelope it may already have arrived on the main sequence and appeared as a visible source with a class III spectral energy distribution. We estimate that, if this possibility is correct, the duration of the class I stage for objects with bolometric luminosities greater than 100 $L_\odot$ is about 9×10^5 yr.

We have also made an attempt to determine the type of young stellar object in the cloud with which molecular outflows are associated. Based on statistical arguments it seems likely that *IRAS* sources tend to be physically associated with regions of high-velocity gas in the cloud. In fact, of *IRAS* sources with bolometric luminosities greater than 50 $L_\odot$, half are associated with high-velocity gas. Assuming that the high-velocity gas is all due to outflows, this suggests that at least half of all luminous young stellar objects go through the outflow phase at some time during their early evolution, and that the birthrate of outflow driving sources in the solar neighborhood is at least 3×10^{-5} kpc^{-2} yr^{-1}. This lower limit on the birthrate, derived without assuming a value for a typical outflow lifetime, is the same as that of 4 $M_\odot$ stars in the solar neighborhood. In addition, about 80% of the luminous ($L_{bol} \geq 50\ L_\odot$) young stellar objects in the cloud are class I objects. As a result it is likely that luminous young stellar objects spend less than 20% of their lifetimes in the class II stage. Since half of the luminous young stellar objects have associated high-velocity gas, these observations suggest that the outflow phase occurs in the earliest stages of pre–main-sequence and protostellar evolution.

We thank John Black, Walt Kailey, and Ian Gatley for useful discussions concerning this paper. This research was supported in part by *IRAS* Guest Investigator grant NAS7-918.

REFERENCES

Adams, F. C., Lada, C. J., and Shu, F. H. 1987, *Ap. J.*, **312**, 788.
———. 1988, *Ap. J.*, **326**, 865.
Adams, F. C., and Shu, F. H. 1986, *Ap. J.*, **308**, 836.
Adams, M. T., Strom, K. M., and Strom, S. E. 1983, *Ap. J. Suppl.*, **53**, 893.
Allen, C. W. 1973, *Astrophysical Quantities* (London: Athlone).
Allen, D. A. 1972, *Ap. J. (Letters)*, **172**, L55.
Bally, J., and Lada, C. J. 1983, *Ap. J.*, **265**, 824.
Beichman, C. A., Neugebauer, G., Habing, H. J., Clegg, P. E., and Chester, T. J. 1985, *IRAS Explanatory Supplement* (Pasadena: Joint *IRAS* Working Group).
Cannon, A. J., and Pickering, E. C. 1918, *Henry Draper Catalogue* (*Annals Astr. Obs. Harvard College*, **92**).
Cohen, M., Harvey, P. M., and Schwartz, R. D. 1985, *Ap. J.*, **296**, 633.
Cohen, M., Harvey, P. M. Schwartz, R. D., and Wilking, B. A. 1984, *Ap. J.*, **278**, 671.
Cohen, M., and Schwartz, R. D. 1983, *Ap. J.*, **265**, 877.
Harvey, P. M., Campbell, M. F., and Hoffmann, W. F. 1977, *Ap. J.*, **215**, 151.
Herbig, G. H. 1954, *Ap. J.*, **119**, 483.
Iijima, T. and Ishida, K. 1978, *Pub. Astr. Soc. Japan*, **30**, 657.
Kleinmann, S. G., Cutri, R. M., Young, E. T., Low, F. J., and Gillet, F. C. 1986, *Explanatory Supplement to the IRAS Serendipitous Survey Catalog* (Pasadena: Joint *IRAS* Working Group).
Lada, C. J. 1985, *Ann. Rev. Astr. Ap.*, **23**, 267.
———. 1987, in *Star Forming Regions*, ed. M. Peimbert and J. Jugaku (Dordrecht: Reidel), p. 1.
Lada, C. J., and Wilking, B. A. 1984, *Ap. J.*, **287**, 610.
Margulis, M., and Lada, C. J. 1986, *Ap. J. (Letters)*, **309**, L87.
Margulis, M., Lada, C. J., and Snell, R. L. 1988, *Ap. J.*, **333**, 316.
Myers, P. C., Heyer, M., Snell, R. L., and Goldsmith, P. F. 1988, *Ap. J.*, **324**, 907.
Ostriker, J. P., Richstone, D. O., and Thuan, T. X. 1974, *Ap. J. (Letters)*, **188**, L87.
Rucinski, S. M. 1985, *A.J.*, **90**, 2321.
Rydgren, A. E., Schmelz, J. T., Zak, D. S., and Vrba, F. J. 1984, *Pub. U.S. Naval Obs.*, **25**, Pt. I.
Sargent, A. I., Van Duinen, R. J., Nordh, H. L., Fridlund, C. V. M., Aalders, J. W. G., and Beintema, D. 1984, *Astr. Ap.*, **135**, 377.
Smithsonian Astrophysical Observatory Star Catalog 1966, (Washington, DC: US Government Printing Office).
Snell, R. L., Huang, Y. L., Dickman, R. L., and Claussen, M. J. 1988, *Ap. J.*, **325**, 853.
Stahler, S. W., Shu, F. H., and Taam, R. E. 1980, *Ap. J.*, **241**, 637.
Vasilevskis, S., Sanders, W. L., and Balz, A. G. A., Jr. 1965, *A.J.*, **70**, 797.
Walker, M. F. 1956, *Ap. J. Suppl.*, **2**, 365.
Warner, J. W., Strom, S. E., and Strom, K. M. 1977, *Ap. J.*, **213**, 427.
Wilking, B. A., Lada, C. J., and Young, E. T. 1989, *Ap. J.*, **340**, 823.
Wynn-Williams, C. G. 1982, *Ann. Rev. Astr. Ap.*, **20**, 587.
Young, E. T., Lada, C. J., and Wilking, B. A. 1986, *Ap. J. (Letters)*, **304**, L45.

C. J. Lada and E. T. Young: Steward Observatory, University of Arizona, Tucson, AZ 85721

M. Margulis: Five College Radio Astronomy Observatory, University of Massachusetts, Amherst, MA 01003

© American Astronomical Society • Provided by the NASA Astrophysics Data System